Research Article

Journal of PeptideScience

Received: 12 April 2012 Revised: 5 July 2012 Accepted: 9 July 2012 Published online in Wiley Online Library: 30 August 2012

(wileyonlinelibrary.com) DOI 10.1002/psc.2441

# Improved anticancer potency by head-to-tail cyclization of short cationic anticancer peptides containing a lipophilic $\beta^{2,2}$-amino acid

Veronika Tørfoss,[a] Johan Isaksson,[b] Dominik Ausbacher,[a] Bjørn-Olav Brandsdal,[b,c] Gøril E. Flaten,[d] Trude Anderssen,[a] Cristiane de A. Cavalcanti-Jacobsen,[a] Martina Havelkova,[a] Leonard T. Nguyen,[e] Hans J. Vogel[e] and Morten B. Strøm[a]*

**We have recently reported a series of synthetic anticancer heptapeptides (H-KKW$\beta^{2,2}$WKK-$NH_2$) containing a central achiral and lipophilic $\beta^{2,2}$-amino acid that display low toxicity against non-malignant cells and high proteolytic stability. In the present study, we have further investigated the effects of increasing the rigidity and amphipathicity of two of our lead heptapeptides by preparing a series of seven to five residue cyclic peptides containing the two most promising $\beta^{2,2}$-amino acid derivatives as part of the central lipophilic core. The peptides were tested for anticancer activity against human Burkitt's lymphoma (Ramos cells), haemolytic activity against human red blood cells (RBC) and cytotoxicity against healthy human lung fibroblast cells (MRC-5). The results demonstrated a considerable increase in anticancer potency following head-to-tail peptide cyclization, especially for the shortest derivatives lacking a tryptophan residue. High-resolution NMR studies and molecular dynamics simulations together with an annexin-V-FITC and propidium iodide fluorescent assay showed that the peptides had a membrane disruptive mode of action and that the more potent peptides penetrated deeper into the lipid bilayer. The need for new anticancer drugs with novel modes of action is demanding, and development of short cyclic anticancer peptides with an overall rigidified and amphipathic structure is a promising approach to new anticancer agents.** 

*Supporting information may be found in the online version of this article.*

**Keywords:** anticancer peptides; beta-amino acid; head-to-tail cyclic peptides; molecular dynamics simulations; structure activity relationship, NMR

## Introduction

According to the American Cancer Society, cancer is the second most common cause of death in the US, only exceeded by heart diseases [1]. Although a number of successful treatments have been established, many anticancer chemotherapeutics are themselves life-threatening because their low preference for malignant cells compared with healthy cells [2]. The need for anticancer drugs with new modes of action is therefore pressing. Among new classes of anticancer drugs being investigated,

* *Correspondence to: Morten B. Strøm, Department of Pharmacy, Faculty of Health Sciences, University of Tromsø, NO-9037 Tromsø, Norway. E-mail: morten.strom@uit.no*

a *Natural Products and Medicinal Chemistry Research Group, Department of Pharmacy, Faculty of Health Sciences, University of Tromsø, NO-9037 Tromsø, Norway*

b *Drug Discovery and Design, Department of Chemistry, Faculty of Science and Technology, University of Tromsø, NO-9037 Tromsø, Norway*

c *Centre of Theoretical and Computational Chemistry, Department of Chemistry, Faculty of Science and Technology, University of Tromsø, NO-9037 Tromsø, Norway*

d *Drug Transport and Delivery Research Group, Department of Pharmacy, Faculty of Health Sciences, University of Tromsø, NO-9037 Tromsø, Norway*

e *Biochemistry Research Group, Department of Biological Sciences, University of Calgary, Calgary, Alberta, Canada, T2N 1N4*

***Abbreviations:*** *CAPs, cationic antimicrobial peptides; Ramos, human Burkitt's lymphoma; RBC, human red blood cells; MRC-5, human embryonic lung fibroblasts; MD, molecular dynamics; NMR, nuclear magnetic resonance; COSY, correlation spectroscopy; NOESY, nuclear overhauser effect spectroscopy; ROESY, rotating frame overhauser effect spectroscopy; TOCSY, total correlation spectroscopy; PyAOP, (7-azabenzotriazol-1-yloxy)tripyrrolidinophosphonium hexafluorophosphate; SDS, sodium dodecyl sulphate; DMPC, 1,2-dimyristoyl-glycero-3-phosphatidyl choline; SUV, small unilamellar vesicles; PCS, photon correlation spectroscopy; TBTC, tributyltin chloride; DMF, N,N-dimethylformamide; DBU, 1,8-diazabicylo[5.4.0]undec-7-ene; HBTU, O-benzotriazole-N,N,N′,N′-tetramethyl-uronium-hexafluorophosphate; HOBt, N-hydroxybenzotriazole; DIPEA, N,N-diisopropylethylamine; TFFH, fluoro-N,N,N′,N′-tetramethylformamidinium hexafluorophosphate; TFA, trifluoroacetic acid; DCM, dichloromethane; TIS, triisopropylsilane; HFIP, 1,1,1,3,3,3-hexafluoro-2-propanol; SPPS, solid phase peptide synthesis; FITC, fluorescein isothiocyanate*

innate immunity peptides or cationic antimicrobial peptides (CAPs) have emerged as promising candidates for cancer treatment [3–5].

CAPs are a structurally diverse class of peptides that includes amphipathic peptides with the ability to kill bacteria, fungi, virus, parasites and cancer cells [3,6]. When exerting their effects on cancer cells, anticancer CAPs are believed to target and disrupt the integrity of the cancer cell membrane, including the cell membranes in multi-drug resistant tumours [7–13]. However, other modes of action have been demonstrated, such as disruption of the mitochondrial membrane, induction of apoptosis and activation of adaptive immunity [14,15]. Because CAPs are not targeting specific extracellular or intracellular receptors, they may avoid countermeasures such as efflux pumps involved in resistance and potentially form a new class of drugs to be injected directly into established tumours [16,17].

Another important aspect favouring development of CAP-based drugs compared with small drug molecules is the tendency of the latter to interact with multiple targets and thereby cause more adverse effects *in vivo* [18,19]. There is, however, a trade-off that has to be met between CAPs and small drug molecules with respect to ensuring both efficient synthesis and optimal pharmacokinetic properties. Developing peptidomimetics by reducing the size of larger anticancer CAPs and introducing unnatural amino acids are thus important strategies for developing new peptide-based chemotherapeutics. There are several examples of use of this approach including anticancer pentadecapeptides, nonapeptides and hexapeptides developed from SAR studies on bovine lactoferricin (LfcinB) and beetle defensins, as well as the small anticancer lipopeptides patented by Shai and Avrahami [15,20–24]. Also, short cyclic peptides have a much better serum stability making them more useful as potential drugs [25].

We have recently demonstrated high anticancer potency of short linear heptapeptides (H-KKW$\beta^{2,2}$WKK-$NH_2$) containing a central achiral and lipophilic $\beta^{2,2}$-amino acid [26]. Especially heptapeptides containing $\beta^{2,2}$-amino acids with two 2-naphthylmethylene or *para*-$CF_3$-benzyl side chains were highly potent against cancer cells and displayed low toxicity against non-malignant cells (side chain structures are shown in Scheme 1). The central lipophilic $\beta^{2,2}$-amino acid is believed to induce turns in peptides, and our studies have shown that the $\beta^{2,2}$-amino acid also protects against proteolytic degradation by trypsin and $\alpha$-chymotrypsin [26].

In the present study, we have further investigated the effects of increasing the rigidity and amphipathicity of our lead heptapeptides by preparing a series of seven to five residue head-to-tail cyclic peptides containing a $\beta^{2,2}$-amino acid with either the two 2-naphthyl-methylene or *para*-$CF_3$-benzyl side chains and compared the anticancer potency and toxicity of the resulting peptides with their linear C-terminal amidated counterparts. The peptides were tested for anticancer activity against human Burkitt's lymphoma (Ramos cells), haemolytic activity against human red blood cells (RBC) and cytotoxicity against healthy human lung fibroblast cells (MRC-5). High-resolution NMR techniques and molecular dynamics (MD) simulations were used to investigate solution conformations and effects upon membrane interaction of three selected peptides, and the mode of action was briefly addressed in an annexin-V-FITC and propidium iodide fluorescent assay.

The results revealed a considerable improvement in anticancer potency against Ramos cells following peptide cyclization, which correlated with changes in secondary conformations, increased rigidity and amphipathicity, and a membrane disruptive mode of action.

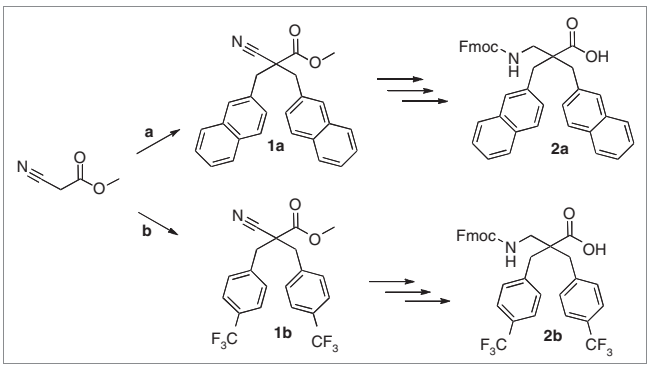


**Scheme 1.** Synthesis of the Fmoc-protected $\beta^{2,2}$-amino acids **2a** and **2b**. **a**: $K_2CO_3$, 2-(bromomethyl)naphthalene. **b**: $K_2CO_3$, 4-(trifluoromethyl)benzyl bromide. The rest of the synthesis is published in Tørfoss *et al.* [26].

## Results and Discussion

### Synthesis

The two Fmoc-$\beta^{2,2}$-amino acids **2a** and **2b** were synthesized as reported earlier except for the initial dialkylation of methyl cyanoacetate (Scheme 1) [26,27]. The dialkylation was previously performed in two steps by using NaOMe as base. By exchanging the nucleophilic base NaOMe with $K_2CO_3$ and adding all reagents in one step, the reactions gave improved yields and avoided the by-products 2-(methoxymethyl)naphthalene and 1-(methoxymethyl)-4-(trifluoromethyl)benzene.

All peptides were synthesized using standard Fmoc-solid phase peptide synthesis on Rink amide MBHA resin for the linear C-terminal amidated peptides and 2-chlorotritylchloride resin for the linear fully Boc-protected peptides to be cyclized. The latter peptides were cyclized under high dilution conditions by using PyAOP as coupling reagent. The cyclization reactions were in general completed after 1–8 h, and hardly any linear peptide was observed. The good yield was likely assisted by the turn-inducing properties of the central $\beta^{2,2}$-amino acid (further results not shown).

### Anticancer Activity

The results revealed that cyclization gave a substantial improvement in anticancer potency, especially when cyclizing the shortest peptides (Table 1). Thus, **c3**, **c4**, **c7** and **c8** were 6 to 11 times more potent against Ramos cancer cells than their linear counterparts. It is also worth noting that almost irrespective of size, charge and lipophilicity, the cyclic peptides' potencies against the Ramos cancer cell line were all within a very narrow range of 8–20 μM, whereas the linear derivatives displayed anticancer potencies in the range 17–226 μM.

Although cyclization of bioactive peptides is a common method for improving the proteolytic stability of peptides, we have recently demonstrated that lipophilic $\beta^{2,2}$-amino acids protect scissile peptide bonds from cleavage in at least two adjacent residues on each side [26]. Thus, the general improvement in anticancer potency following cyclization of the peptides presented here was more likely due to structural effects, than due to increased proteolytic stability.

When investigating the linear peptides, deletion of a cationic lysine residue from the lead heptapeptides **1** and **5** had little effect on anticancer potency, as shown for the resulting peptides

  

Journal of PeptideScience

**Table 1.** Anticancer potency of linear and (**cyclic**) peptides against Ramos ($IC_{50}$ in μM), toxicity against human erythrocytes (RBC, $EC_{50}$ in μM) and healthy human lung fibroblast cells (MRC-5, $IC_{50}$ in μM). All linear peptides were *C*-terminally amidated, and the results for the cyclic peptides are shown in (**bold**)

| Entry | Sequence | Anticancer activity | | Toxicity | | | | Rt[f] | |
|---|---|---|---|---|---|---|---|---|---|
| | | Ramos[a,c] | | RBC[b, d] | | MRC-5[a, e] | | | |
| $\beta^{2,2}$(2-Nal-$CH_2$-) | | | | | | | | | |
| **1** (**c1**) | KKW$\beta^{2,2}$WKK | $22 \pm 5$[g] | (**10** ± **2**) | 425[g] | (**87**) | $58 \pm 6$[g] | (**10** ± **1**) | 11.9 | (**15.3**) |
| **2** (**c2**) | KW$\beta^{2,2}$WKK | 17.1 ± 0.6 | (**7.9** ± **0.3**) | 256 | (**31**) | 30 ± 2 | (**13** ± **1**) | 13.2 | (**19.1**) |
| **3** (**c3**) | KK$\beta^{2,2}$WKK | 92 ± 2 | (**15** ± **2**) | — | (**256**) | — | (**30** ± **2**) | 10.2 | (**13.9**) |
| **4** (**c4**) | KW$\beta^{2,2}$KK | 99 ± 15 | (**12.6** ± **0.6**) | — | (**110**) | 283 ± 14 | (**23.5** ± **0.7**) | 11.4 | (**16.6**) |
| $\beta^{2,2}$(p-$CF_3$-Bzl-) | | | | | | | | | |
| **5** (**c5**) | KKW$\beta^{2,2}$WKK | $23 \pm 3$[g] | (**11** ± **2**) | —[g] | (**141**) | $140 \pm 9$[g] | (**26** ± **3**) | 12.2 | (**15.5**) |
| **6** (**c6**) | KW$\beta^{2,2}$WKK | 26 ± 2 | (**8** ± **1**) | 316 | (**36**) | 85 ± 4 | (**23** ± **1**) | 13.6 | (**17.6**) |
| **7** (**c7**) | KK$\beta^{2,2}$WKK | 157 ± 30 | (**16** ± **5**) | — | — | — | (**31** ± **2**) | 13.4 | (**14.4**) |
| **8** (**c8**) | KW$\beta^{2,2}$KK | 226 ± 21 | (**20** ± **2**) | — | (**298**) | — | (**53** ± **2**) | 12.0 | (**15.6**) |

[a]Highest concentrations tested were 500 μg/ml.
[b]Highest concentrations tested were 1000 μg/ml.
[c]Human Burkitt's lymphoma B lymphocyte.
[d]Human red blood cells.
[e]Normal human embryonic lung fibroblast cells (ATCC CCL-171).
[f]Retention time on an analytical RP-HPLC column.
[g]Previously published in Tørfoss *et al.* [26]. The symbol '—' denotes no detectable activity ($IC_{50}$ or $EC_{50}$) within the concentration range tested.

**2** and **6**. However, when deleting a tryptophan residue from the same lead heptapeptides, a marked decrease in potency was observed for the resulting peptides **3** and **7** (Table 1). Noteworthy, cyclization of the linear hexapeptides **3** and **7** into **c3** and **c7** restored the anticancer potency to the same level as for the most potent linear heptapeptides. A similar increase in anticancer potency was observed in case of cyclization of the linear pentapeptides **4** and **8** into the cyclic pentapeptides **c4** and **c8**, which all were lacking both a tryptophan and a lysine residue.

Although deletion of a lysine residue was somewhat tolerated, deleting a tryptophan residue had a negative impact on anticancer potency (Table 1). Tryptophan is known from structural studies of membrane proteins to be prominent in the water–phospholipid interface region of membranes and has a particular preference for inserting into this complex region of phospholipid membranes through its quadropolar moment [11,28–30]. Tryptophan residues can also interact with other aromatic systems through π–π-stacking interactions and thereby contribute to secondary conformations through face-to-face or face-to-edge stacking depending on the aromatic system it interacts with [31]. The present results also implied that the positive effect of flanking the $\beta^{2,2}$-amino acids by two tryptophan residues was eliminated when one of them was deleted (**3**, **4**, **7** and **8**). The recovered potency upon cyclization (**c3**, **c4**, **c7** and **c8**) may be the result of the amphipathic conformation being reinforced without the need of this tryptophan effect.

Also when inspecting the retention times (Rt) on an analytical RP-HPLC column, almost regardless of net cationic charge, the linear peptides eluted much faster (Rt: 10.2–13.6 min) than the cyclic peptides (Rt: 13.9–19.1 min), which reflected conformational differences in the interaction between the peptides and the stationary phase of the RP-HPLC column (Table 1).

When inspecting the influence of the two $\beta^{2,2}$-amino acid structures, there was little difference in anticancer potency among the linear peptides containing a $\beta^{2,2}$-amino acid with two 2-naphthyl-methylene side chains compared with the linear peptides containing two *para*-$CF_3$-benzyl side chains, as long as the lipophilic core sequence – W$\beta^{2,2}$W – was intact. However, without this lipophilic cluster and for peptides with a lipophilic core consisting of $\beta^{2,2}$W (**3** and **7**) or W$\beta^{2,2}$ (**4** and **8**), the 2-naphthyl-methylene side chains seemed more efficient with respect to anticancer potency. In case of the cyclic peptides, the differences in potency with respect to $\beta^{2,2}$-amino acid side chain structures was much less evident.

### Toxicity

Among the linear peptides, only peptides **1**, **2** and **6** displayed detectable haemolytic activity within the concentration range tested (i.e. up to 1000 μg/ml), whereas all the cyclic peptides, except for **c7**, displayed measurable haemolytic activity (Table 1). Because RBCs are non-metabolizing cells without a nucleus, the peptides were also tested for cytotoxicity against MRC-5 cells. The peptides were in general more cytotoxic against MRC-5 cells than RBC, but among the linear peptides, **5** was sixfold more potent against Ramos cancer cells compared with MRC-5 cells, whereas among the cyclic peptides, **c6** displayed the highest preference for Ramos cancer cells by showing almost threefold higher potency than against MRC-5 cells. Thus, the toxicity of the peptides against RBC and MRC-5 cells followed the same pattern as the anticancer potencies, in which the linear peptides were less toxic than their cyclic counterparts. However, all peptides investigated were in general more potent against Ramos cancer cells than against RBC and MRC-5 cells.

### Structural Investigations by NMR and MD Simulations

The lead heptapeptide **5** was among the four most potent linear peptides, but as described earlier, deletion of a tryptophan (**7**) resulted in almost a sevenfold drop in anticancer activity that was completely recovered through cyclization (**c7**) (Table 1). Because **5**, **7** and **c7** also were non-haemolytic, they were selected for studies by NMR and MD simulations to investigate structural effects related to their anticancer potencies. Liposome



  

dispersions of 1,2-dimyristoyl-glycero-3-phosphatidyl choline (DMPC) were used as membrane model system, and the peptide structures in liposomes were compared with the natural state of the peptides in deuterated water. The peptides were also studied in deuterated SDS, which is often used for larger peptides and proteins as membrane mimic to induce folds that are more likely to be similar to the ones adopted in biological membranes. To investigate the peptide structures, we focused on the interactions between the lipophilic side chains, that is, the *para*-$CF_3$-benzyl groups and tryptophan residue(s), and the lysine residues.

*Aqueous solution*

The NMR spectra of all three peptides **5**, **7** and **c7** were first acquired in $D_2O$ for assignment and examination of structural properties of the peptides in an aqueous environment. The structural effects of cyclization were revealed by inspection of the ROESY cross peaks between lysines and the two *para*-$CF_3$-benzyl groups in **7** and **c7**, and showed that the more deshielded *para*-$CF_3$-benzyl group in **c7** became separated from the lysine residues and lost detectable cross relaxation with any of the lysine resonances compared with the linear peptide **7** (details in Figures S3 and S4 in the Supporting Information). Furthermore, the more shielded *para*-$CF_3$-benzyl group in **c7** displayed a less efficient cross relaxation with the lysine residues, resulting in generally weaker cross peaks. Both these observations reflected a separation of the charged and lipophilic moieties resulting in high amphipathic character of the cyclic peptide **c7** compared with its linear counterpart **7**.

The NMR results were supported by MD simulations in water, which showed decreased benzyl-lysine contacts in **c7** compared with both **5** and **7** when the intramolecular distances from the two *para*-$CF_3$-benzyl groups to each lysine residue were plotted versus simulation time (details in Figures S13a,c,e and S14a,c,e in the Supporting Information). The ability of both the linear peptides **5** and **7** to position their lysine residues near the hydrophobic moieties allowed them, at least partially, to hide the hydrophobic parts from the surrounding water by stacking the aliphatic lysine side chain over the $\pi$-surfaces. These observations provided a rational explanation to the 1 min shorter retention time in RP-HPLC of **7** compared with its cyclic counterpart **c7** (Table 1). This effect was however not as pronounced as has been previously reported for shorter antimicrobial peptides [32]. Therefore, the solubility effects originating from the conformation in water alone, even if it contributed positively, cannot be expected to fully account for the almost tenfold increase in anticancer potency upon cyclization of **7** to **c7**. The internal dynamics in solution also became significantly slowed down for the $\alpha$-protons upon cyclization. The $T_1/T_2$ relaxation quota went from ~3 to ~30, owing to a decrease in $T_2$ relaxation time that could likely be attributed to slow motions of the cyclic backbone in the microsecond to nanosecond regime. This was also reflected in less frequent structural fluctuations of **c7** compared with **5** and **7** in the MD trajectories (see Figure S14a,c,e in the Supporting Information).

*SDS micelles*

Peptides **5**, **7** and **c7** were also studied by NMR in SDS micelles. NOESY spectra (100 ms) revealed that the more active peptides, **5** and **c7**, showed only weak or undetectable cross peaks between the *para*-$CF_3$-benzyl groups and any of the lysine residues (see Figures S5 and S7 in the Supporting Information), whereas the less active peptide **7** maintained clearly detectable cross peaks also in SDS (see Figure S6 in the Supporting Information). This indicated that **5** and **c7** adopted a more amphipathic conformation in SDS micelles where the charged lysine residues and the hydrophobic *para*-$CF_3$-benzyl groups spent very little time near each other.

*Liposome dispersion*

The peptides **5**, **7** and **c7** were titrated into DMPC liposome dispersions in $D_2O$ to study their effects on lipid bilayers. In case of the least potent peptide **7**, high quality spectra were obtained at a final peptide concentration of 3.6 mM (Figure S8 in the Supporting Information). NOESY buildup revealed that **7** maintained contacts between the aliphatic protons of the lysine residues and the *para*-$CF_3$-benzyl group protons. This implied that **7** did not adopt a fully amphipathic conformation normally associated with membrane penetration, even though the peptide clearly was associated to the liposomes, as confirmed by short $T_2$ relaxation and weak NOESY cross peaks to the lipid choline resonances at longer mixing times (100 ms). Of notice, during the 50 ns of MD simulations, **7** associated to the membrane surface but without separating all lysine residues from the *para*-$CF_3$-benzyl side chains and by only inserting one of the two *para*-$CF_3$-benzyl groups into the membrane, thereby supporting the results from the NMR studies (see Figures 2b and 14d in the Supporting Information).

The more active peptides, **5** and **c7**, were however not tolerated in the liposome dispersion studies up to the desired concentrations of ~3 mM, resulting in extensive line broadening, coalescence of the outside and inside choline peaks into one signal and a general loss of signal intensity for the lipid signals (see Figures S11 and S12 in the Supporting Information). Determination of liposome size by photon correlation spectroscopy (PCS) after exceeding the critical peptide concentration for peptide **c7** showed that the average diameter of the liposomes had increased from approximately 30 nm to 65 nm in addition to a small population with diameters of 240 nm, indicating that **c7** disturbed the integrity of the liposomes and caused them to fuse. In this respect, it is worth noting that the trend of peptide tolerance of the liposomes correlated well with the anticancer potency of each peptide (Figure S12). This supported the view that the peptides had a direct mode of action against the lipid bilayer integrity, as there were no potential biological target proteins present in the liposomes except for the phospholipid bilayer itself.

The MD simulations of peptides **5**, **7** and **c7** with the peptides placed at the water–phospholipid interface region revealed that **5** and **c7** were able to penetrate deeper into the lipid bilayer during the 50 ns simulation than **7**, which stayed associated with the outer membrane surface (Figures 1 and 2). The most striking difference was in the way the peptides inserted into the membrane. The two linear peptides, **5** and **7**, both inserted the $\beta^{2,2}$-amino acid vertically, thereby burying only one of the *para*-$CF_3$-benzyl groups deeply into the bilayer (see Figure 2). In contrast, the cyclic **c7** flipped the entire $\beta^{2,2}$-amino acid down, penetrating the membrane with the entire lipophilic core. The major difference between the active, **5**, and the inactive, **7**, linear peptides was the additional tryptophan of **5** that appeared to facilitate entry and penetrated deeply into the membrane. In **7**, the neighbouring lysine residue instead followed the $\beta^{2,2}$-amino acid into the membrane, thereby placing the positively charged side chain in an unfavourable uncharged environment (see Figure 2). The MD simulations thus suggested that the tryptophan residues in **5** played an important role in the penetration process as well as in determining the depth of peptide insertion into the lipid bilayer. It is worth noting that the fluctuation of the lysine side chains was not slowed down by the

  

Journal of PeptideScience

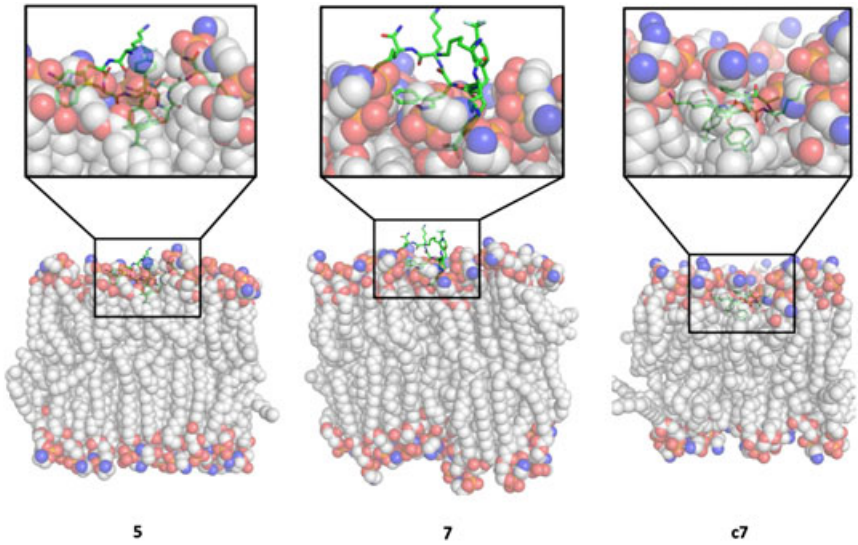


**Figure 1.** Representative snapshots of **5**, **7** and **c7** (green sticks) as observed in the MD simulations of the peptides in a lipid bilayer (semi-transparent spheres).

association of **7** to the bilayer but continued to fluctuate freely in sharp contrast to the lysine residues of both **5** and **c7** where the MD trajectory clearly showed that the internal dynamics was restricted by the membrane environment (see Figure S13b,d,f in the Supporting Information).

It was also apparent from the MD simulations that **c7** was able to cause greater distortion of the lipid acyl chains than the linear counterpart (Figures S14–S17 in the Supporting Information). Although **7** also attached to the membrane surface and interacted favourably with the membrane throughout the simulations, the hydrophobic residues did not fully enter the membrane, and significantly less distorted lipid acyl chains were observed.

### Annexin-V-FITC and Propidium Iodide Fluorescent Assay

An annexin-V-FITC and propidium iodide fluorescent assay combined with flow cytometry was used to investigate the mechanism of cell death caused by the peptides [33]. In brief, FITC labelled annexin-V does not permeate the cell membrane and thus only binds to phosphatidylserine exposed on the outer leaflet of the cell membrane of intact cells or with phosphatidylserine on the inner leaflet of late disrupted cells. It is thus used both to detect translocation of phosphatidylserine from the inner to the outer leaflet of cell membranes during early stages of apoptosis and to detect late apoptotic/necrotic cells. Propidium iodide is a polar non-membrane permeable red fluorescent dye that intercalates DNA when the integrity of the cell membrane is destroyed and can thereby be used for detecting cells in late apoptotic/necrotic stages. By measuring the fluorescence from annexin-V-FITC and propidium iodide, any noticeable differences in the mechanism of action may be revealed [34]. The results of the annexin-V-FITC and propidium iodide fluorescent assay are exemplified by the heptapeptides **1/c1** and **5/c5** (Figure 3). Results for all peptides are shown in Figure S18 in the Supporting Information.

The results indicated a direct membrane disruptive mechanism of action by the simultaneous increase in fluorescence of both annexin-V-FITC and propidium iodide (Figure 3). Thus, all treated cells seemed to move directly from the living cell cluster (lower left quadrant) to the necrotic/late apoptotic cell cluster (top right quadrant), without first appearing in the apoptotic cell cluster (top left quadrant). The simultaneous increase in fluorescent intensity from annexin-V-FITC and propidium iodide indicated increased permeability of both reagents and additional binding of annexin-V-FITC also to inner leaflet phosphatidylserine. The results therefore suggested a direct cell membrane disrupting mode of action for both the linear and cyclic peptides at their $IC_{50}$ concentration. There seemed, however, to be a difference in the efficiency of the cyclic peptides compared with the linear peptides, especially for peptides with a $\beta^{2,2}$-amino acid with two naphthyl-methylene side chains. As evident by the higher amount of cells in the necrotic top right quadrant, the cyclic peptides, **c1** and **c5**, seemed to more efficiently cause cancer cell necrosis compared with the linear peptides **1** and **5**.

### Concluding Remarks

In addition to a minimum requirement of bulk and cationic charge, an important prerequisite for high potency of membrane active peptides is the ability to adopt an amphipathic conformation upon interaction with cancer cell membranes, that is, with the lipophilic and cationic residues well separated [3,35]. The lead heptapeptides **1** and **5** were originally designed to form an amphipathic wedge-shaped conformation upon interaction with cancer cell membranes consisting of the lipophilic core sequence W$\beta^{2,2}$W flanked by cationic lysine residues [26]. In the present study, we have shown how shorter, similarly potent peptides without the lipophilic core structure were prepared by head-to-tail cyclization, as exemplified by the promising peptide **c7**.

Through studies by NMR spectroscopy and MD simulations on the three selected peptides **5**, **7** and **c7**, we have furthermore demonstrated how the more potent peptides **5** and **c7** had a more profound amphipathic conformation both in water, SDS micelles and DMPC bilayers compared with the less active peptide **7**. This emphasized the importance of the core sequence W$\beta^{2,2}$W as facilitator of an amphipathic structure in linear peptides because **5**, with an intact core sequence, was more structured in contact with membranes as opposed to **7** where the core sequence was reduced to $\beta^{2,2}$W. By cyclizing **7** into **c7**, a more structured amphipathic conformation was reintroduced followed by nearly tenfold increased anticancer potency.



  

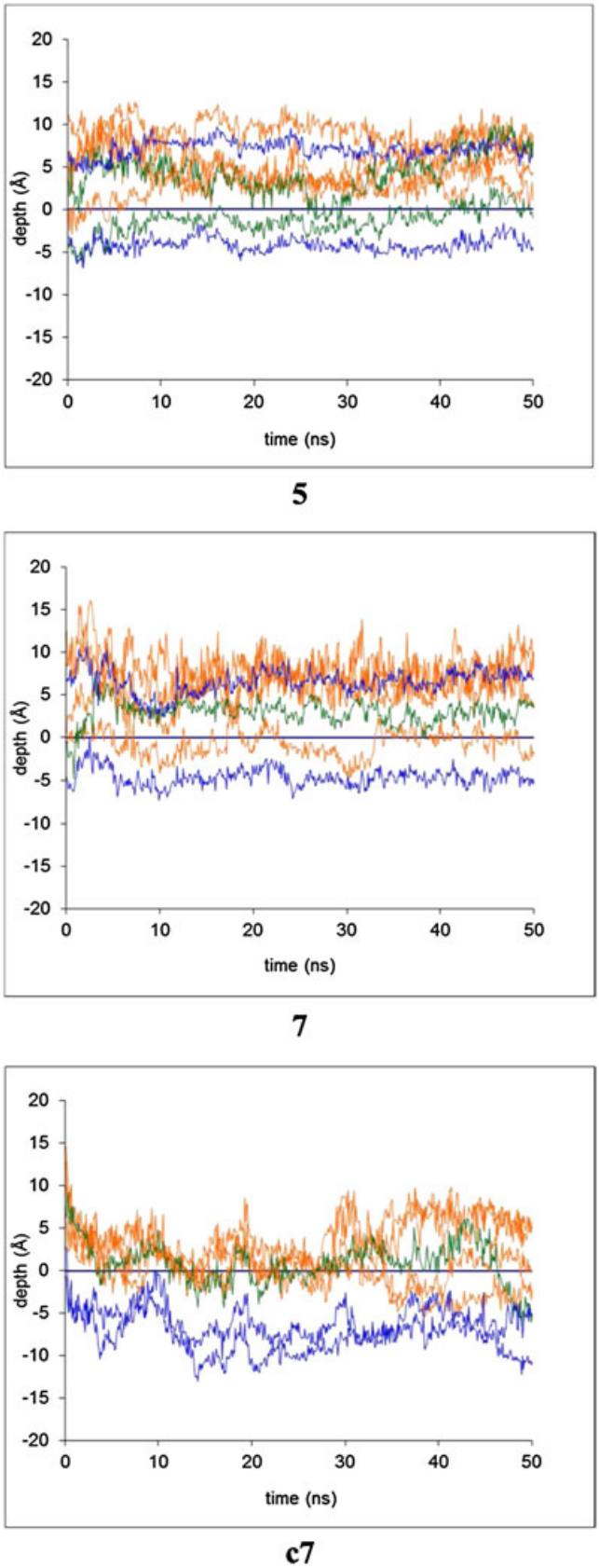


**Figure 2.** The depth of peptide penetration below the bilayer surface defined as the phosphate plane; *para*-CF3-benzyl side chains (blue), tryptophan residue(s) (green) and lysine residues (orange), plotted versus simulation time for peptides **5** (top), **7** (middle) and **c7** (bottom). The surface line is represented by a dark blue line through zero.

Additionally, both MD simulations, where the more active peptides were buried deeper into the membrane giving more distortion of the lipid acyl chains, and annexin-V-FITC/propidium iodide fluorescent assays indicated a direct membrane disruptive mode of action for these peptides. The MD simulations also revealed that although **5** and **c7** were similarly active, their structural mechanism differed. **c7** was able to accommodate both $\beta^{2,2}$-amino acid side chains deep into the membrane, giving more membrane distortion than **5** where only one $\beta^{2,2}$-amino acid side chain and one tryptophan entered the membrane (Figure 2).

Because of the high anticancer activity and low haemolytic activity, the linear peptide **5** and the cyclic peptide **c7** are promising leads for development of future anticancer drugs. For future studies, it would be interesting to investigate if such short peptides are able to cause activation of adaptive immunity *in vivo* as has been reported for much larger peptides and on a molecular level synthesize diastereomeric peptides by including one or more D-amino acids to further tune the selectivity against cancer cells compared with non-malignant cells [15,36].

## Experimental Section

Synthesis of Fmoc-$\beta^{2,2}$-amino acids and linear peptides were performed as reported earlier, except the initial disubstitution of methyl cyanoacetate [26,27]. All chemicals were purchased from Sigma-Aldrich and used without further purification.

### Synthesis of 1a

Methyl cyanoacetate (1 eq.) was dissolved in DMF (0.6 M), and $K_2CO_3$ (2 eq.) was added. The suspension was stirred for 1 h at rt before 2-(bromomethyl)naphthalene (2.2 eq.) dissolved in DMF (1.2 M) was slowly added. The reaction mixture was stirred overnight before it was reduced to approximately 5 ml, and the crude product was extracted from water with EtOAc. The crude product was isolated as brown oil (99%) and used in following syntheses without further purification.

### Synthesis of 1b

**1b** was synthesized by the same method as **1a**, replacing 2-bromomethyl)naphthalene with 4-(trifluoromethyl)benzyl bromide. The crude product was isolated as brown oil (98%) and used in following syntheses without further purification.

### Synthesis of Linear Peptides 1–8

The synthesis was based on standard Fmoc solid phase peptide synthesis [37]. *Swelling of the resin*: The Rink amide MBHA resin was swelled in DMF for 1 h and washed with DMF. *Fmoc-removal*: The Fmoc-protection group was removed with DMF : DBU : Piperidine 48 : 1 : 1 (3 × 5 min) before the resin was washed with DMF. *Coupling of amino acids to the deprotected resin*: Fmoc-Lys(Boc)-OH or Fmoc-Trp(Boc)-OH (4 eq.) HOBt hydrate (4 eq.), HBTU (3.96 eq.) and DIPEA (8 eq.) were dissolved in DMF, allowed to preactivate for 15 min and added to the resin. The mixture was stirred for 1 h before it was filtered off, and the resin was washed with DMF followed by Fmoc-removal. *Coupling of the $\beta^{2,2}$-amino acids to the deprotected resin*: Fmoc-$\beta^{2,2}$-aa-OH (2 eq.), TFFH (1.9 eq.) and DIPEA (8 eq.) were dissolved inn DMF, allowed to preactivate for 15 min and added to the resin. The mixture was stirred overnight before it was filtered off, and the resin was washed with DMF followed by addition of another preactivated mixture of Fmoc-$\beta^{2,2}$-aa-OH (2 eq.), TFFH (1.9 eq.) and DIPEA (8 eq.) in

  

Journal of PeptideScience

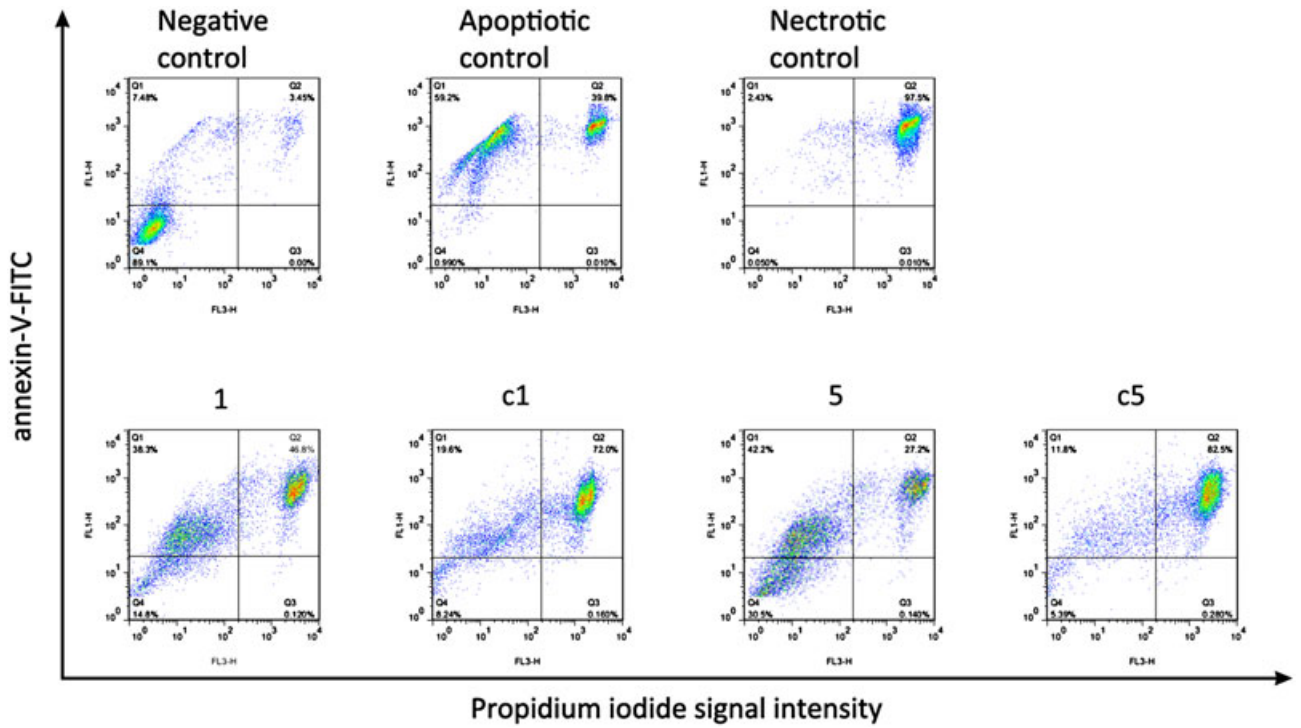


**Figure 3.** Representative dotplots showing annexin-V-FITC staining versus propidium iodide staining. Ramos cells treated with peptides **1**, **c1**, **5** and **c5**, and incubated at their IC50 values for 4 h, as in the MTT assay, were subsequently stained with annexin-V-FITC and propidium iodide, and analysed by flow cytometry. Untreated Ramos cancer cells were used as negative control, Ramos cancer cells treated with 1 μM TBTC were used as apoptotic control and Ramos cells treated with 10 μM TBTC were used as necrotic control.

DMF. The mixture was stirred for 2 h before it was filtered off, and the resin was washed with DMF followed by Fmoc-removal. *Cleavage from the resin*: After the last coupling and Fmoc-removal, the resin was washed with DCM and allowed to dry. A mixture of TFA : TIS : water (95 : 2.5 : 2.5) (10 ml) was added to the reaction tubes, and the suspension was stirred for 2 h before the peptide solution was collected. This procedure was repeated twice, with stirring times of 10 min each. The combined peptide solutions were evaporated to dryness under reduced pressure, and the residue was precipitated with diethyl ether and washed with diethyl ether. The peptides were purified by RP-HPLC to a purity of >95% and lyophilized.

### Synthesis of Cyclic Peptides c1–c8

The Fmoc solid phase peptide synthesis was performed as for the linear peptides, except for the swelling of the resin, the attachment of the first amino acid and the cleavage from the resin. *Swelling of resin and attachment of the first amino acid*: The 2-chlorotritylchloride resin was swelled in DCM for 1 h and washed with DCM. Fmoc-Lys(Boc)-OH (4 eq.) and DIPEA (8 eq.) were dissolved in DCM and added to the resin. The mixture was stirred for 1 h before it was filtered off, and the resin was washed with DCM. The remaining active sites of the resin were capped using MeOH in a mixture of DCM : MeOH : DIPEA 80 : 15 : 5 (2 × 10 min), and the resin was washed first with DCM and then DMF. *Cleavage from the resin*: After the last coupling and Fmoc-removal, the resin was washed with DCM and allowed to dry. A mixture of HFIP : DCM (3 : 7) was added, and the mixture was stirred for 45 min before the peptide solution was collected. The procedure was repeated twice more with stirring times of 10 min. The combined peptide solutions were evaporated to dryness under reduced pressure. *Cyclization*: The linear peptides were dissolved in DMF : DCM 1 : 1 (0.18 mM), and DIPEA (2 eq.) was added and allowed to preactivate for 15 min before PyAOP (2 eq.) was added, and the solution was slowly stirred for 1–8 h. The solvents were removed under reduced pressure, and the remaining peptide was dissolved in TFA : TIS : $H_2O$ 95 : 2.5 : 2.5 (20 ml) and stirred for 3 h. Finally, the solvents were evaporated under reduced pressure, and the peptides were purified by RP-HPLC to a purity of >95% and lyophilized.

### MTT-assays, Haemolytic Assays and Annexin-assays

MTT-assays, haemolytic assays and annexin-assays were performed as described in an earlier publication from the group [26].

### NMR

The NMR spectra in water and in 1,2-dimyristoyl-glycero-3-phosphatidyl choline (DMPC) liposomes were acquired on a Varian/Agilent Inova spectrometer operating at 599.934 and 150.863 MHz for $^{1}H$ and $^{13}C$, respectively, by using a cryogenically cooled inverse detection HCN probe with enhanced proton channel (2nd generation).

For assignment, 2D phase insensitive gradient selected COSY, gradient selected edited HSQC and absolute value HMBC (adiabatic versions), and ROESY (adiabatic version) were acquired with typical resolution of 1440 × 200 complex data points and eight transients. All spectra were acquired at 298 K in $D_2O$ (Sigma-Aldrich).

DMPC liposome dispersions 50 mg/ml in 10 mM phosphate buffer in $D_2O$, pH 7.0, were made using the film hydration method [38]. Probe sonication (Vibracell high intensity ultrasonic processor from Sonics and Materials, Newtown, CT, USA) was used in 2 min cycles to prepare small unilamellar vesicles (SUVs) with a mean number weighted diameter of about 30 nm. The size of the liposomes was measured by photon correlation spectroscopy (PCS) using a Submicron Particle Sizer 370 (PSS Nicomp Particle



  

Sizing Systems, Santa Barbara, CA, USA). Sample preparation and measuring conditions were as described earlier [39]. Three cycles of 15 min each were performed.

The TOCSY with 38 ms mixing time and NOESY spectra with mixing times of 25, 50 and 100 ms were acquired for samples in liposome dispersions. For relaxation measurements, standard inversion recovery was used to measure $T_1$ and Carr–Purcell–Meiboom–Gill experiment to measure $T_2$. Peaks were integrated and fitted to exponential decay functions by using Mnova 7.1.1.

The NMR spectra in SDS micelles were acquired at 298 K on a Bruker Avance 700-MHz spectrometer equipped with a 5-mm TBI 3-axis gradient probe. TOCSY and NOESY spectra were collected using mixing times of 60 and 100 ms, respectively, and the samples were prepared using about 2.5 mM peptide and 250 mM perdeuterated SDS in $D_2O$.

### Molecular Dynamics Simulations

The peptides with $Cl^-$ as counter ions were initially built using Maestro, version 9.2 [40] and relaxed using the UFF minimizer. The OPLS2005 force field [41,42] was used for all calculations with the Desmond program package [43–45]. The simulations were performed using an orthorombic box where the boundaries were controlled by a buffer distance of 20 Å between the solute and the box edges. Peptide-solvent simulations were conducted using water described with the TIP3P model [46]. Peptide-membrane simulations were conducted with a model system consisting of a 1-palmitoyl-2-oleoyl-glycero-3-phosphoethanolamine (POPE) membrane and explicit TIP3P [46] water molecules. The production phase consisted of 50 ns with sampling of structures every 1.2 ps.

All simulations were carried out with the NPT ensemble at 300 K and 1 atm. The NPT ensemble was calculated with the Nose–Hoover thermostat method [47,48] with a relaxation time of 1.0 ps and a frequency update every second step, and the Martyna–Tobias–Klein barostat method [49], using isotropic coupling with a relaxation time of 2.0 ps and a compressibility of $4.5 \times 10^{-5}$ (1/bar). Short range Coulombic interactions were treated with a cut-off radius of 9 Å. Long range interactions were treated with the smooth Particle Mesh Ewald method [50] with a tolerance of $10^{-9}$. Simulations of 50 ns were carried out using the reference system propagator algorithm (RESPA) time-stepping scheme [51] with time steps set to 2 fs for bonded and near atoms and 6 fs for far atoms. Heavy atom–hydrogen covalent bonds were constrained using SHAKE [52] with a tolerance of $10^{-8}$ with a maximum of eight iterations.

For trajectory analysis, snapshots were dumped every 20 frames after equilibration, resulting in a total of 520 structure per trajectory where the *z*-axis was translated to the normal of the bilayer surface. Shell/gawk scripts were used to extract inter-atom distances and vectors. The bilayer surface was defined as a plane through the average position of the phosphates along the *z*-axis, and the *para*-$CF_3$-benzyls were represented by the $CF_3$ carbon, the lysines by the side chain nitrogen and the tryptophan by the nearest of the two edge carbons, 5 and 6.

### General Analysis

The HRMS spectra were recorded on a Waters Micromass LCT Premier time-of-flight (TOF) mass spectrometer equipped with an electrospray ion source and analysed using MassLynx v4.1 software. The samples were introduced to the mass spectrometer by using a Waters 2795 analytical HPLC with an XTerra MS 3.5 μm $C_{18}$ reversed phase column (2.1 × 50 mm) (Waters). The mobile phase consisted of different combinations of MilliQ water and acetonitrile, both containing 0.1% formic acid, and a gradient running for 5 min was used. Leucine–enkephalin was infused through the reference probe and used as lock mass for internal calibrations throughout the data acquisitions. All data were acquired in the positive ion mode. $^1H$ and $^{13}C$ NMR experiments were recorded on a Varian 400 NMR spectrometer or a Varian 600 NMR spectrometer with $CDCl_3$ or $CD_3OD$ as solvents and analysed using Vnmr software. Chemical shifts are expressed in parts per million (ppm, δ) and referred to the solvent signal [53]. The preparative HPLC system consisted of a Waters 600 E System controller, a Waters In-line Degasser, a Waters 717 auto sampler and a Model 2487 dual λ Absorbance Detector controlled by Empower Pro software. A SunFire Prep OBD, 5 μm $C_{18}$ RP column (19 × 250 mm) (Waters) was used. The absorbance detector was operated at 214 nm. The mobile phase was different combinations of 5% acetonitrile in MilliQ water (A) and 95% acetonitrile in MilliQ water (B), both containing 0.1% TFA, and the flow rate was 15 ml/min. The analytical HPLC system consisted of a Waters 2695 Separations Module and a Waters 996 Photodiode Array Detector controlled by Empower Pro software. A SunFire 5 μm $C_{18}$ RP column (4.6 × 250 mm) was used for purity analysis. An YMC-Pack Pro 5 μm $C_{18}$ RP column (4.6 × 250 mm) was used for Rt analysis. The compounds were analysed at wavelengths 214 and 254 nm with the PDA detector spanning from wavelength 210 to 310 nm The mobile phase was different combinations of 5% acetonitrile in MilliQ water (A) and 95% acetonitrile in MilliQ water (B), both containing 0.1% TFA, using a gradient of 10%–60% B and a flow rate of 1 ml/min.

*H-Lys-Lys-Trp-(2,2-di(naphthalen-2-ylmethyl)-3-amino-propionic acid)-Trp-Lys-Lys-$NH_2$* (***1***) was synthesized and characterized as **10f** in [26]

*H-Lys-Lys-Trp-(2,2-di(naphthalen-2-ylmethyl)-3-amino-propionic acid)-Trp-Lys-$NH_2$* (***2***) was synthesized by SPPS using **2a** as the Fmoc-$\beta^{2,2}$-amino acid and isolated as white powder after lyophilization (14%). ESI-TOF-MS$^+$: $[M+H]^+$ observed: 1125.6445, calculated: 1125.6402. HPLC-UV (PDA Max Plot 190–800 nm): Gradient: 20%–60% B over 20 min; $R_t$: 13.15 min; Purity: 98.4%. $^1H$ NMR (600 MHz, $H_2O:D_2O$ 9:1) δ 9.95 (s, 1H), 9.76 (s, 1H), 7.72 (dd, *J* = 11.3, 5.5 Hz, 3H), 7.57 (d, *J* = 7.7 Hz, 1H), 7.55–7.47 (m, 3H), 7.44 (d, *J* = 8.5 Hz, 1H), 7.41–7.30 (m, 6H), 7.27 (d, *J* = 8.1 Hz, 1H), 7.19 (d, *J* = 8.2 Hz, 1H), 7.17 (s, 1H), 7.10 (d, *J* = 3.6 Hz, 2H), 7.04 (dt, *J* = 19.2, 7.5 Hz, 2H), 6.98 (t, *J* = 7.3 Hz, 2H), 6.90 (d, *J* = 8.9 Hz, 2H), 6.83 (t, *J* = 7.4 Hz, 1H), 6.69 (s, 2H), 6.60 (d, *J* = 8.5 Hz, 1H), 4.18 (q, *J* = 6.2 Hz, 1H), 3.86 (t, *J* = 6.5 Hz, 1H), 3.82 (dd, *J* = 12.8, 6.4 Hz, 1H), 3.78 (dd, *J* = 13.7, 6.9 Hz, 1H), 3.16–3.03 (m, 3H), 2.98 (d, *J* = 10.7 Hz, 1H), 2.85–2.74 (m, 2H), 2.74–2.65 (m, 4H), 2.62 (d, *J* = 14.4 Hz, 1H), 2.56 (s, 3H), 2.48 (d, *J* = 14.5 Hz, 1H), 2.43 (t, *J* = 7.4 Hz, 2H), 2.32 (d, *J* = 14.6 Hz, 1H), 1.74–1.64 (m, 2H), 1.50 (dt, *J* = 14.8, 7.6 Hz, 1H), 1.44–1.29 (m, 5H), 1.14 (ddd, *J* = 24.5, 15.4, 7.4 Hz, 8H), 1.00–0.89 (m, 1H), 0.78–0.61 (m, 2H).

*H-Lys-Lys-Trp-(2,2-di(naphthalen-2-ylmethyl)-3-amino-propionic acid)-Lys-Lys-$NH_2$* (***3***) was synthesized by SPPS using **2a** as the Fmoc-$\beta^{2,2}$-amino acid and isolated as white powder after lyophilization (27%). ESI-TOF-MS$^+$: $[M+H]^+$ observed: 1067.6609, calculated: 1067.6559. HPLC-UV (PDA Max Plot 190–800 nm): Gradient: 20%–60% B over 20 min; $R_t$: 10.19 min; Purity: 99.7%. $^1H$ NMR (600 MHz, $H_2O:D_2O$ 9:1) δ 9.77 (s, 1H), 8.01 (t, *J* = 5.1 Hz, 1H), 7.84 (d, *J* = 6.5 Hz, 1H), 7.77 (d, *J* = 7.2 Hz, 2H), 7.72 (d, *J* = 7.8 Hz, 1H), 7.64 (dd, *J* = 13.7, 8.2 Hz, 2H), 7.52–7.34 (m, 10H), 7.29 (s, 1H), 7.19 (d, *J* = 8.2 Hz, 1H), 7.14 (d, *J* = 8.0 Hz, 1H), 7.06 (d, *J* = 8.5 Hz, 1H), 7.03 (t, *J* = 7.6 Hz, 1H), 6.92 (s, 1H), 6.88

  

Journal of PeptideScience

(t, $J$ = 7.6 Hz, 1H), 6.86 (s, 1H), 6.80 (d, $J$ = 8.5 Hz, 1H), 4.35 (dd, $J$ = 12.1, 6.2 Hz, 2H), 3.92 (dd, $J$ = 13.4, 6.5 Hz, 1H), 3.87 (d, $J$ = 6.5 Hz, 1H), 3.83 (t, $J$ = 6.5 Hz, 1H), 3.24 (d, $J$ = 14.6 Hz, 1H), 3.20–2.99 (m, 6H), 2.91 (dd, $J$ = 14.6, 7.9 Hz, 1H), 2.76 (dt, $J$ = 19.6, 7.5 Hz, 4H), 2.49 (t, $J$ = 7.4 Hz, 2H), 2.39 (t, $J$ = 7.3 Hz, 2H), 1.71–1.61 (m, 2H), 1.61–1.34 (m, 9H), 1.34–1.12 (m, 9H), 1.08 (dt, $J$ = 15.7, 7.9 Hz, 2H), 0.94–0.86 (m, 1H), 0.86–0.77 (m, 1H).

*H-Lys-Lys-(2,2-di(naphthalen-2-ylmethyl)-3-amino-propionic acid)-Trp-Lys-NH$_2$ (**4**)* was synthesized by SPPS using **2a** as the Fmoc-$\beta^{2,2}$-amino acid and isolated as white powder after lyophilization (27%). ESI-TOF-MS$^+$: $[M+H]^+$ observed: 939.5564, calculated: 939.5609. HPLC-UV (PDA Max Plot 190–800 nm): Gradient: 20%–60% B over 20 min; $R_t$: 11.36 min; Purity: 99.7%. $^1$H NMR (600 MHz, $H_2O:D_2O$ 9 : 1) δ 10.02 (s, 1H), 7.90 (d, $J$ = 6.6 Hz, 1H), 7.75 (d, $J$ = 7.7 Hz, 2H), 7.68 (dd, $J$ = 19.7, 8.2 Hz, 2H), 7.63 (d, $J$ = 7.7 Hz, 1H), 7.56 (dd, $J$ = 18.6, 8.1 Hz, 2H), 7.45–7.36 (m, 5H), 7.36–7.24 (m, 5H), 7.16 (s, 1H), 7.01 (dt, $J$ = 12.9, 6.7 Hz, 4H), 6.86 (s, 1H), 6.77 (d, $J$ = 8.4 Hz, 1H), 3.86 (dd, $J$ = 14.0, 6.9 Hz, 2H), 3.72 (dd, $J$ = 12.8, 6.3 Hz, 1H), 3.20–3.03 (m, 4H), 2.83 (d, $J$ = 14.9 Hz, 1H), 2.74 (d, $J$ = 14.1 Hz, 1H), 2.59 (t, $J$ = 7.3 Hz, 2H), 2.53 (t, $J$ = 7.1 Hz, 2H), 2.48 (d, $J$ = 15.0 Hz, 1H), 2.42 (d, $J$ = 14.2 Hz, 1H), 2.24 (s, 2H), 1.70 (dd, $J$ = 15.0, 7.8 Hz, 2H), 1.46–1.22 (m, 8H), 1.18 (dd, $J$ = 14.9, 7.5 Hz, 2H), 1.13–1.04 (m, 3H), 1.04–0.95 (m, 1H), 0.95–0.85 (m, 1H), 0.57–0.48 (m, 1H), 0.48–0.39 (m, 1H).

*H-Lys-Lys-Trp-(2,2-di(4-[trifluoromethyl]benzyl)-3 amino-propionic acid)-Trp-Lys-Lys-NH$_2$ (**5**)* was synthesized and characterized as **10e** in [26].

*H-Lys-Lys-Trp-(2,2-di(4-[trifluoromethyl]benzyl)-3-amino-propionic acid)-Trp-Lys-NH$_2$ (**6**)* was synthesized by SPPS using **2b** as the Fmoc-$\beta^{2,2}$-amino acid and isolated as white powder after lyophilization (34%). ESI-TOF-MS$^+$: $[M+H]^+$ observed: 1161.5872, calculated: 1161.5837. HPLC-UV (PDA Max Plot 190–800 nm): Gradient: 20%–60% B over 20 min; $R_t$: 13.57 min; Purity: 95.1%. $^1$H NMR (600 MHz, $H_2O:D_2O$ 9 : 1) δ 10.05 (s, 1H), 9.90 (s, 1H), 8.67 (d, $J$ = 5.8 Hz, 1H), 7.97 (d, $J$ = 6.5 Hz, 1H), 7.87 (d, $J$ = 7.2 Hz, 1H), 7.51 (d, $J$ = 7.7 Hz, 1H), 7.43 (s, 1H), 7.28 (t, $J$ = 8.4 Hz, 3H), 7.23 (t, $J$ = 7.8 Hz, 3H), 7.16 (d, $J$ = 7.7 Hz, 2H), 7.12 (s, 2H), 7.10–7.02 (m, 2H), 7.00–6.88 (m, 4H), 6.64 (d, $J$ = 7.8 Hz, 2H), 6.57 (d, $J$ = 7.8 Hz, 2H), 4.26 (d, $J$ = 6.5 Hz, 1H), 4.00 (dd, $J$ = 13.7, 6.9 Hz, 1H), 3.94 (dd, $J$ = 12.7, 6.2 Hz, 1H), 3.88 (t, $J$ = 6.4 Hz, 1H), 3.12 (dd, $J$ = 14.1, 5.7 Hz, 1H), 3.08–3.01 (m, 1H), 2.95 (dd, $J$ = 14.6, 5.9 Hz, 1H), 2.85 (dd, $J$ = 14.9, 8.3 Hz, 1H), 2.81–2.70 (m, 5H), 2.70–2.61 (m, 3H), 2.57 (d, $J$ = 14.5 Hz, 2H), 2.47 (d, $J$ = 14.5 Hz, 1H), 2.30 (d, $J$ = 14.4 Hz, 1H), 2.20 (d, $J$ = 14.8 Hz, 1H), 1.78–1.69 (m, 3H), 1.65–1.53 (m, 3H), 1.38 (dt, $J$ = 14.4, 7.1 Hz, 4H), 1.29–1.13 (m, 5H), 1.13–0.97 (m, 3H).

*H-Lys-Lys-Trp-(2,2-di(4-[trifluoromethyl]benzyl)-3-amino-propionic acid)-Lys-Lys-NH$_2$ (**7**)* was synthesized by SPPS using **2b** as the Fmoc-$\beta^{2,2}$-amino acid and isolated as white powder after lyophilization (37%). ESI-TOF-MS$^+$: $[M+H]^+$ observed: 1103.5925, calculated: 1103.5993. HPLC-UV (PDA Max Plot 190–800 nm): Gradient: 20%–60% B over 20 min; $R_t$: 11.37 min; Purity: 99.8%. $^1$H NMR (600 MHz, $H_2O:D_2O$ 9 : 1) δ 9.95 (s, 1H), 8.53 (d, $J$ = 6.7 Hz, 1H), 8.09 (d, $J$ = 7.0 Hz, 1H), 8.06 (d, $J$ = 6.5 Hz, 1H), 7.97 (t, $J$ = 5.0 Hz, 1H), 7.54 (d, $J$ = 6.2 Hz, 1H), 7.47 (s, 1H), 7.39 (d, $J$ = 7.9 Hz, 3H), 7.29 (d, $J$ = 8.2 Hz, 1H), 7.14 (d, $J$ = 7.9 Hz, 2H), 7.11–7.02 (m, 4H), 6.98 (t, $J$ = 7.5 Hz, 1H), 6.95 (s, 1H), 6.73 (d, $J$ = 7.8 Hz, 2H), 4.43 (dd, $J$ = 13.6, 6.8 Hz, 1H), 4.30 (q, $J$ = 6.8 Hz, 1H), 4.09 (q, $J$ = 6.7 Hz, 1H), 3.99 (q, $J$ = 6.6 Hz, 1H), 3.86 (t, $J$ = 6.2 Hz, 1H), 3.14–3.06 (m, 2H), 3.02–2.93 (m, 2H), 2.93–2.76 (m, 8H), 2.76–2.62 (m, 4H), 1.72 (d, $J$ = 6.2 Hz, 2H), 1.66–1.48 (m, 10H), 1.48–1.40 (m, 4H), 1.35–1.08 (m, 8H).

*H-Lys-Lys-(2,2-di(4-[trifluoromethyl]benzyl)-3-amino-propionic acid)-Trp-Lys-NH$_2$ (**8**)* was synthesized by SPPS using **2b** as the Fmoc-$\beta^{2,2}$-amino acid and isolated as white powder after lyophilization (50%). ESI-TOF-MS$^+$: $[M+H]^+$ observed: 975.5048, calculated: 975.5044. HPLC-UV (PDA Max Plot 190–800 nm): Gradient: 20%–60% B over 20 min; $R_t$: 11.96 min; Purity: 99.9%. $^1$H NMR (600 MHz, $H_2O:D_2O$ 9 : 1) δ 10.09 (d, $J$ = 1.7 Hz, 1H), 8.73 (d, $J$ = 5.8 Hz, 1H), 8.15 (d, $J$ = 6.7 Hz, 1H), 7.53 (d, $J$ = 7.9 Hz, 1H), 7.44–7.38 (m, 3H), 7.34 (d, $J$ = 7.6 Hz, 3H), 7.29 (d, $J$ = 8.1 Hz, 1H), 7.17 (s, 1H), 7.11 (d, $J$ = 6.6 Hz, 1H), 7.04 (t, $J$ = 7.5 Hz, 1H), 6.98 (t, $J$ = 7.5 Hz, 1H), 6.93 (d, $J$ = 8.1 Hz, 3H), 6.76 (d, $J$ = 8.0 Hz, 2H), 3.98 (dd, $J$ = 14.2, 6.6 Hz, 1H), 3.90 (br s, 2H), 3.16 (dd, $J$ = 14.1, 5.8 Hz, 1H), 3.08 (dd, $J$ = 13.9, 10.8 Hz, 1H), 2.92 (dd, $J$ = 14.1, 4.7 Hz, 1H), 2.82 (dd, $J$ = 14.6, 5.7 Hz, 2H), 2.79 (br s, 1H), 2.75–2.67 (m, 4H), 2.64 (dd, $J$ = 14.2, 9.1 Hz, 2H), 2.38 (d, $J$ = 14.6 Hz, 1H), 2.29 (d, $J$ = 14.1 Hz, 1H), 1.76 (dt, $J$ = 11.6, 5.9 Hz, 2H), 1.64–1.56 (m, 1H), 1.57–1.48 (m, 4H), 1.45 (dt, $J$ = 14.9, 7.5 Hz, 3H), 1.41–1.33 (m, 2H), 1.33–1.18 (m, 4H), 1.18–1.09 (m, 1H), 0.90–0.74 (m, 2H).

*c(Lys-Lys-Trp-(2,2-di(naphthalen-2-ylmethyl)-3-amino-propionic acid)-Trp-Lys-Lys) (**c1**)* was synthesized using **2a** as the Fmoc-$\beta^{2,2}$-amino acid and isolated as white powder after lyophilization (47%). ESI-TOF-MS$^+$: $[M+H]^+$ observed: 1237.7096, calculated: 1237.7096. HPLC-UV (PDA Max Plot 190–800 nm): Gradient: 20%–60% B over 20 min; $R_t$: 15.28 min; Purity: 99.9%. $^1$H NMR (600 MHz, $H_2O:D_2O$ 9 : 1) δ 9.93 (s, 1H), 9.59 (s, 1H), 8.26 (s, 1H), 8.13 (br s, 1H), 7.73 (s, 1H), 7.60 (s, 5H), 7.47 (s, 2H), 7.37 (d, $J$ = 6.5 Hz, 5H), 7.32 (s, 2H), 7.25 (d, $J$ = 7.0 Hz, 3H), 7.16 (d, $J$ = 28.5 Hz, 2H), 7.02 (s, 3H), 6.96 (s, 2H), 6.88 (s, 2H), 6.72 (s, 1H), 6.60 (s, 1H), 4.38 (s, 1H), 4.01 (s, 2H), 3.70 (br s, 1H), 3.53 (s, 1H), 3.33 (br s, 1H), 3.17–2.95 (m, 4H), 2.86 (br s, 2H), 2.81 (br s, 1H), 2.68 (br s, 8H), 2.45 (br s, 3H), 1.84–1.63 (m, 3H), 1.63–1.47 (m, 5H), 1.47–1.33 (m, 6H), 1.28 (br s, 2H), 1.23–1.13 (m, 1H), 1.13–0.93 (m, 7H).

*c(Lys-Lys-Trp-(2,2-di(naphthalen-2-ylmethyl)-3-amino-propionic acid)-Trp-Lys) (**c2**)* was synthesized using **2a** as the Fmoc-$\beta^{2,2}$-amino acid and isolated as white powder after lyophilization (28%). ESI-TOF-MS$^+$: $[M+H]^+$ observed: 1108.6163, calculated: 1108.6137. HPLC-UV (PDA Max Plot 190–800 nm): Gradient: 20%–60% B over 20 min; $R_t$: 19.09 min; Purity: 99.6%. $^1$H NMR (400 MHz, $CD_3OD$) δ 7.84 (t, $J$ = 8.7 Hz, 3H), 7.70 (t, $J$ = 8.4 Hz, 5H), 7.61 (s, 1H), 7.56–7.43 (m, 6H), 7.34 (dd, $J$ = 8.2, 4.6 Hz, 2H), 7.20 (d, $J$ = 8.0 Hz, 1H), 7.16–7.06 (m, 3H), 7.04–6.94 (m, 3H), 4.25 (t, $J$ = 8.3 Hz, 1H), 4.00 (t, $J$ = 7.5 Hz, 1H), 3.81 (br s, 1H), 3.69 (dd, $J$ = 11.3, 3.3 Hz, 1H), 3.50–3.33 (m, 2H), 3.27–3.11 (m, 4H), 3.07 (dd, $J$ = 13.7, 8.5 Hz, 1H), 2.98 (d, $J$ = 15.3 Hz, 1H), 2.83–2.75 (m, 3H), 2.75–2.57 (m, 5H), 2.57–2.46 (m, 1H), 2.05–1.75 (m, 4H), 1.66–1.25 (m, 9H), 1.16–0.99 (m, 2H), 0.91 (dd, $J$ = 29.3, 13.8 Hz, 2H), 0.83–0.71 (m, 1H).

*c(Lys-Lys-Trp-(2,2-di(naphthalen-2-ylmethyl)-3-amino-propionic acid)-Lys-Lys) (**c3**)* was synthesized using **2a** as the Fmoc-$\beta^{2,2}$-amino acid and isolated as white powder after lyophilization (7%). ESI-TOF-MS$^+$: $[M+H]^+$ observed: 1050.6298, calculated: 1050.6293. HPLC-UV (PDA Max Plot 190–800 nm): Gradient: 20%–60% B over 20 min; $R_t$: 13.85 min; Purity: 99.9%. $^1$H NMR (600 MHz, $H_2O:D_2O$ 9 : 1) δ 9.90 (s, 1H), 8.19 (s, 1H), 7.94 (s, 1H), 7.88–7.78 (m, 1H), 7.70 (d, $J$ = 7.1 Hz, 1H), 7.65 (d, $J$ = 5.9 Hz, 1H), 7.55 (d, $J$ = 7.1 Hz, 2H), 7.51–7.43 (m, 3H), 7.40–7.28 (m, 5H), 7.25 (s, 1H), 7.17 (d, $J$ = 8.1 Hz, 1H), 7.06 (s, 1H), 7.01 (s, 1H), 6.94 (t, $J$ = 7.2 Hz, 1H), 6.86 (d, $J$ = 7.0 Hz, 1H), 6.81 (d, $J$ = 7.6 Hz, 1H), 6.72 (dd, $J$ = 15.9, 8.6 Hz, 3H), 4.31 (s, 1H), 3.93 (br s, 1H), 3.75 (dd, $J$ = 11.2, 6.5 Hz, 1H), 3.21 (d, $J$ = 11.3 Hz, 1H), 3.14 (d, $J$ = 16.6 Hz, 1H), 2.86 (d, $J$ = 13.5 Hz, 1H), 2.83–2.71 (m, 10H), 2.68–2.54 (m, 5H), 1.69–1.52 (m, 2H), 1.52–1.16 (m, 16H), 1.16–0.83 (m, 6H).



  

*c(Lys-Lys-(2,2-di(naphthalen-2-ylmethyl)-3-amino-propionic acid)-Trp-Lys) (**c4**)* was synthesized using **2a** as the Fmoc-$\beta^{2,2}$-amino acid and isolated as white powder after lyophilization (43%). ESI-TOF-MS$^+$: $[M+H]^+$ observed: 922.5302, calculated: 922.5343. HPLC-UV (PDA Max Plot 190–800 nm): Gradient: 20%–60% B over 20 min; $R_t$: 16.57 min; Purity: 99.9%. $^1$H NMR (700 MHz, $H_2O:D_2O$ 9 : 1): δ 10.15 (s, 1H), 8.69 (d, *J* = 6.4 Hz, 1H), 7.93 (dd, *J* = 19.6, 8.4 Hz, 2H), 7.85 (d, *J* = 7.0 Hz, 2H), 7.80 (t, *J* = 8.6 Hz, 2H), 7.68 (d, *J* = 6.9 Hz, 1H), 7.64–7.54 (m, 5H), 7.52 (d, *J* = 8.6 Hz, 2H), 7.49 (s, 1H), 7.45 (s, 1H), 7.37 (d, *J* = 8.9 Hz, 1H), 7.25 (d, *J* = 9.0 Hz, 1H), 7.13 (d, *J* = 9.8 Hz, 1H), 7.10–7.01 (m, 3H), 6.49 (s, 1H), 4.55 (d, *J* = 6.4 Hz, 1H), 4.21 (s, 1H), 3.93 (d, *J* = 7.4 Hz, 1H), 3.84 (d, *J* = 6.8 Hz, 1H), 3.36 (d, *J* = 5.3 Hz, 1H), 3.29 (dd, *J* = 15.8, 8.9 Hz, 2H), 3.24–3.07 (m, 4H), 3.03 (br s, 3H), 2.92–2.80 (m, 3H), 2.43 (s, 1H), 1.84 (s, 2H), 1.74 (dd, *J* = 17.0, 8.8 Hz, 2H), 1.68–1.58 (m, 2H), 1.54 (dd, *J* = 16.2, 7.6 Hz, 2H), 1.46 (br s, 2H), 1.41–1.24 (m, 3H), 1.24–1.00 (m, 3H), 0.72 (br s, 1H), 0.54 (br s, 1H).

*c(Lys-Lys-Trp-(2,2-di(4-[trifluoromethyl]benzyl)-3 amino-propionic acid)-Trp-Lys-Lys) (**c5**)* was synthesized using **2b** as the Fmoc-$\beta^{2,2}$-amino acid and isolated as white powder after lyophilization (19%). ESI-TOF-MS$^+$: $[M+H]^+$ observed: 1272.6572, calculated: 1272.6521. HPLC-UV (PDA Max Plot 190–800 nm): Gradient: 20%–60% B over 20 min; $R_t$: 15.49 min; Purity: 99.9%. $^1$H NMR (600 MHz, $H_2O:D_2O$ 9 : 1) δ 10.00 (s, 1H), 9.91 (s, 1H), 8.44 (s, 1H), 8.40 (s, 1H), 8.31 (br s, 1H), 7.84 (d, *J* = 6.2 Hz, 1H), 7.67 (s, 1H), 7.53 (dd, *J* = 17.3, 8.0 Hz, 2H), 7.46–7.30 (m, 7H), 7.27 (s, 1H), 7.16 (d, *J* = 8.2 Hz, 1H), 7.15–6.98 (m, 5H), 6.96–6.84 (m, 3H), 6.63 (d, *J* = 7.1 Hz, 1H), 4.18–4.04 (m, 2H), 3.93 (q, *J* = 6.7 Hz, 1H), 3.81 (s, 1H), 3.24–3.12 (m, 1H), 3.09 (dd, *J* = 14.5, 5.0 Hz, 2H), 3.02–2.90 (m, 1H), 2.87–2.66 (m, 11H), 2.66–2.49 (m, 4H), 2.26 (d, *J* = 13.8 Hz, 1H), 1.83–1.66 (m, 5H), 1.63 (d, *J* = 6.4 Hz, 2H), 1.57 (br s, 1H), 1.52–1.41 (m, 5H), 1.41–1.32 (m, 2H), 1.32–1.24 (m, 1H), 1.24–1.17 (m, 3H), 1.12 (br d, *J* = 6.0 Hz, 5H).

*c(Lys-Lys-Trp-(2,2-di(4-[trifluoromethyl]benzyl)-3-amino-propionic acid)-Trp-Lys) (**c6**)* was synthesized using **2b** as the Fmoc-$\beta^{2,2}$-amino acid and isolated as white powder after lyophilization (28%). ESI-TOF-MS$^+$: $[M+H]^+$ observed: 1144.5519, calculated: 1144.5571. HPLC-UV (PDA Max Plot 190–800 nm): Gradient: 20%–60% B over 20 min; $R_t$: 17.64 min; Purity: 99.5%. $^1$H NMR (700 MHz, $H_2O:D_2O$ 9 : 1) δ 8.48 (s, 1H), 8.23 (s, 1H), 8.10 (s, 1H), 7.67 (d, *J* = 6.8 Hz, 2H), 7.63–7.39 (m, 9H), 7.33 (s, 1H), 7.28–7.02 (m, 8H), 6.96 (s, 1H), 4.47 (s, 1H), 4.21–4.11 (m, 1H), 4.06–3.94 (m, 1H), 3.52–3.44 (m, 1H), 3.43–3.39 (m, 1H), 3.34–3.26 (m, 1H), 3.26–3.16 (m, 3H), 3.09–2.68 (m, 11H), 2.52–2.44 (m, 1H), 1.97–1.87 (m, 2H), 1.87–1.76 (m, 1H), 1.75–1.32 (m, 9H), 1.32–1.06 (m, 5H), 1.01 (br s, 1H).

*c(Lys-Lys-Trp-(2,2-di(4-[trifluoromethyl]benzyl)-3-amino-propionic acid)-Lys-Lys) (**c7**)* was synthesized using **2b** as the Fmoc-$\beta^{2,2}$-amino acid and isolated as white powder after lyophilization (30%). ESI-TOF-MS$^+$: $[M+H]^+$ observed: 1086.5759, calculated: 1086.5728. HPLC-UV (PDA Max Plot 190–800 nm): Gradient: 20%–60% B over 20 min; $R_t$: 14.35 min; Purity: 99.9%. $^1$H NMR (600 MHz, $H_2O:D_2O$ 9 : 1) δ 10.11 (s, 1H), 8.29 (s, 1H), 8.11 (s, 1H), 7.96 (d, *J* = 6.8 Hz, 1H), 7.40 (d, *J* = 8.0 Hz, 3H), 7.36–7.28 (m, 5H), 7.18 (s, 1H), 7.11 (t, *J* = 7.6 Hz, 1H), 7.07 (s, 1H), 7.02 (t, *J* = 6.9 Hz, 3H), 6.88 (d, *J* = 7.6 Hz, 2H), 4.05 (dd, *J* = 13.9, 6.4 Hz, 1H), 4.00 (s, 1H), 3.93 (s, 1H), 3.84 (dd, *J* = 13.6, 7.2 Hz, 1H), 3.21 (d, *J* = 8.8 Hz, 1H), 3.16 (dd, *J* = 14.8, 6.1 Hz, 1H), 3.06 (d, *J* = 14.2 Hz, 1H), 2.94 (dd, *J* = 14.7, 8.4 Hz, 1H), 2.90–2.69 (m, 12H), 2.63 (d, *J* = 13.8 Hz, 1H), 1.77–1.63 (m, 3H), 1.63–1.55 (m, 3H), 1.55–1.38 (m, 10H), 1.31–1.23 (m, 1H), 1.23–1.12 (m, 5H), 1.08 (dd, *J* = 16.1, 8.9 Hz, 2H).

*c(Lys-Lys-(2,2-di(4-[trifluoromethyl]benzyl)-3-amino-propionic acid)-Trp-Lys) (**c8**)* was synthesized using **2b** as the Fmoc-$\beta^{2,2}$-amino acid and isolated as white powder after lyophilization (26%). ESI-TOF-MS$^+$: $[M+H]^+$ observed: 958.4817, calculated: 958.4778. HPLC-UV (PDA Max Plot 190–800 nm): Gradient: 20%–60% B over 20 min; $R_t$: 15.55 min; Purity: 99.7%. $^1$H NMR (600 MHz, $H_2O:D_2O$ 9 : 1) δ 10.02 (s, 1H), 8.62 (d, *J* = 5.5 Hz, 1H), 8.39 (d, *J* = 3.9 Hz, 1H), 8.31 (d, *J* = 5.5 Hz, 1H), 7.60 (dd, *J* = 13.6, 7.5 Hz, 1H), 7.52 (d, *J* = 7.6 Hz, 2H), 7.48 (d, *J* = 8.0 Hz, 1H), 7.43 (d, *J* = 7.9 Hz, 2H), 7.40 (s, 1H), 7.31 (dd, *J* = 14.2, 8.1 Hz, 1H), 7.17–7.07 (m, 3H), 7.07–6.91 (m, 2H), 6.83 (s, 1H), 6.73 (s, 1H), 4.42 (dd, *J* = 13.8, 7.5 Hz, 1H), 4.22–4.14 (m, 1H), 4.09 (d, *J* = 4.7 Hz, 1H), 3.91 (dd, *J* = 14.9, 6.6 Hz, 1H), 3.68 (dd, *J* = 14.0, 5.8 Hz, 1H), 3.27 (ddd, *J* = 63.7, 14.2, 5.5 Hz, 1H), 3.16–3.02 (m, 2H), 2.92–2.69 (m, 7H), 2.65 (s, 2H), 2.59 (s, 1H), 1.68 (d, *J* = 3.4 Hz, 1H), 1.62–1.42 (m, 6H), 1.42–1.10 (m, 6H), 1.10–0.82 (m, 4H), 0.82–0.72 (m, 1H).

**Acknowledgements**

The project was supported by the KOSK II grant 185141/V30 from the Norwegian Research Council (NFR). Funding was also provided by the Alberta Cancer Foundation. We thank Dr Espen Hansen (Marbio, University of Tromsø) for providing help in acquiring the HRMS spectra and Prof. Øystein Rekdal (Department of Medical Biology, University of Tromsø) for supplying the Ramos and MRC-5 cells.

## References

1 AmericanCancerSociety. *Cancer Facts & Figures 2011*. American Cancer Society: Atlanta, 2011.
2 Smith LL, Brown K, Carthew P, Lim C-K, Martin EA, Styles J, White INH. Chemoprevention of breast cancer by tamoxifen: Risks and opportunities. *Crit. Rev. Toxicol.* 2000; **30**: 571–594. DOI: 10.1080/10408440008951120
3 Hoskin DW, Ramamoorthy A. Studies on anticancer activities of antimicrobial peptides. *Biochim. Biophys. Acta, Biomembr.* 2008; **1778**: 357–375.
4 Schweizer F. Cationic amphiphilic peptides with cancer-selective toxicity. *Eur. J. Pharmacol.* 2009; **625**: 190–194.
5 Riedl S, Zweytick D, Lohner K. Membrane-active host defense peptides—challenges and perspectives for the development of novel anticancer drugs. *Chem. Phys. Lipids* 2011; **164**: 766–781. DOI: 10.1016/j.chemphyslip.2011.09.004
6 Hancock REW, Diamond G. The role of cationic antimicrobial peptides in innate host defences. *Trends Microbiol.* 2000; **8**: 402–410.
7 Johnstone SA, Gelmon K, Mayer LD, Hancock RE, Bally MB. *In vitro* characterization of the anticancer activity of membrane-active cationic peptides. I. Peptide-mediated cytotoxicity and peptide-enhanced cytotoxic activity of doxorubicin against wild-type and p-glycoprotein over-expressing tumor cell lines. *Anti Cancer Drug Des.* 2000; **15**: 151–160.
8 Cruciani RA, Barker JL, Durell SR, Raghunathan G, Guy HR, Zasloff M, Stanley EF. Magainin 2, a natural antibiotic from frog skin, forms ion channels in lipid bilayer membranes. *Eur. J. Pharmacol.* 1992; **226**: 287–296.
9 Ohsaki Y, Gazdar AF, Chen H-C, Johnson BE. Antitumor activity of magainin analogues against human lung cancer cell lines. *Cancer Res.* 1992; **52**: 3534–3538.
10 Kim S, Kim SS, Bang YJ, Kim SJ, Lee BJ. *In vitro* activities of native and designed peptide antibiotics against drug sensitive and resistant tumor cell lines. *Peptides* 2003; **24**: 945–953.
11 Chan DI, Prenner EJ, Vogel HJ. Tryptophan- and arginine-rich antimicrobial peptides: structures and mechanisms of action. *Biochim. Biophys. Acta, Biomembr.* 2006; **1758**: 1184–1202.
12 Giuliani A, Pirri G, Nicoletto S. Antimicrobial peptides: an overview of a promising class of therapeutics. *Cent. Eur. J. Biol.* 2007; **2**: 1–33.
13 Giuliani A, Pirri G, Bozzi A, Di Giulio A, Aschi M, Rinaldi A. Antimicrobial peptides: natural templates for synthetic membrane-active compounds. *Cell. Mol. Life Sci.* 2008; **65**: 2450–2460. DOI: 10.1007/s00018-008-8188-x

  

14 Eliassen LT, Berge G, Leknessund A, Wikman M, Lindin I, Løkke C, Ponthan F, Johnsen JI, Sveinbjørnsson B, Kogner P, Flægstad T, Rekdal Ø. The antimicrobial peptide, lactoferricin B, is cytotoxic to neuroblastoma cells *in vitro* and inhibits xenograft growth *in vivo*. *Int. J. Cancer* 2006; **119**: 493–500.
15 Berge G, Eliassen L, Camilio K, Bartnes K, Sveinbjørnsson B, Rekdal Ø. Therapeutic vaccination against a murine lymphoma by intratumoral injection of a cationic anticancer peptide. *Cancer Immunol. Immun.* 2010; **59**: 1285–1294. DOI: 10.1007/s00262-010-0857-6
16 Peschel A, Sahl H-G. The co-evolution of host cationic antimicrobial peptides and microbial resistance. *Nat. Rev. Micro.* 2006; **4**: 529–536.
17 Perron GG, Zasloff M, Bell G. Experimental evolution of resistance to an antimicrobial peptide. *Proc. R. Soc. B: Biol. Sci.* 2006; **273**: 251–256. DOI: 10.1098/rspb.2005.3301
18 Leach AR, Hann MM. Molecular complexity and fragment-based drug discovery: ten years on. *Curr. Opin. Chem. Biol.* 2011; **15**: 489–496. DOI: 10.1016/j.cbpa.2011.05.008
19 Overington JP, Al-Lazikani B, Hopkins AL. How many drug targets are there? *Nat. Rev. Drug Discovery* 2006; **5**: 993–996.
20 Iwasaki T, Ishibashi J, Tanaka H, Sato M, Asaoka A, Taylor D, Yamakawa M. Selective cancer cell cytotoxicity of enantiomeric 9-mer peptides derived from beetle defensins depends on negatively charged phosphatidylserine on the cell surface. *Peptides* 2009; **30**: 660–668.
21 Tomita M, Takase M, Bellamy W, Shimamura S. A review: the active peptide of lactoferrin. *Acta Paediatr. Japon.* 1994; **36**: 585–591.
22 Richardson A, de Antueno R, Duncan R, Hoskin DW. Intracellular delivery of bovine lactoferricin's antimicrobial core (RRWQWR) kills T-leukemia cells. *Biochem. Biophys. Res. Commun.* 2009; **388**: 736–741.
23 Shai Y, Avrahami D. Antimicrobial and anticancer lipopeptides. WO2004110341A2, 2004.
24 Eliassen LT, Haug BE, Berge G, Rekdal Ø. Enhanced antitumour activity of 15-residue bovine lactoferricin derivatives containing bulky aromatic amino acids and lipophilic N-terminal modifications. *J. Pept. Sci.* 2003; **9**: 510–517.
25 Nguyen LT, Chau JK, Perry NA, de Boer L, Zaat SAJ, Vogel HJ. Serum stabilities of short tryptophan- and arginine-rich antimicrobial peptide analogs. *PLoS One* 2010; **5**: e12684. DOI: 10.1371/journal.pone.0012684
26 Tørfoss V, Ausbacher DA, Cavalcanti-Jacobsen CdA, Hansen T, Brandsdal B-O, Havelkova M, Strøm MB. Synthesis of anticancer heptapeptides containing a unique lipophilic $\beta^{2,2}$-amino acid building block. *J. Pept. Sci.* 2012; **18**: 170–176.
27 Hansen T, Alst T, Havelkova M, Strøm MB. Antimicrobial activity of small β-Peptidomimetics based on the pharmacophore model of short cationic antimicrobial peptides. *J. Med. Chem.* 2010; **53**: 595–606. DOI: 10.1021/jm901052r
28 Yau W-M, Wimley WC, Gawrisch K, White SH. The preference of tryptophan for membrane interfaces. *Biochem. – US* 1998; **37**: 14713–14718. DOI: 10.1021/bi980809c
29 Persson S, Antoinette Killian J, Lindblom G. Molecular ordering of interfacially localized tryptophan analogs in ester- and ether-lipid bilayers studied by 2 H-NMR. *Biophys. J.* 1998; **75**: 1365–1371.
30 Rekdal Ø, Haug BE, Kalaaji M, Hunter HN, Lindin I, Israelsson I, Solstad T, Yang N, Brandl M, Mantzilas D, Vogel HJ. Relative spatial positions of tryptophan and cationic residues in helical membrane-active peptides determine their cytotoxicity. *J. Biol. Chem.* 2012; **287**: 233–244. DOI: 10.1074/jbc.M111.279281
31 Samanta U, Pal D, Chakrabarti P. Packing of aromatic rings against tryptophan residues in proteins. *Acta Crystallogr. D* 1999; **55**: 1421–1427.
32 Isaksson J, Brandsdal BO, Engqvist M, Flaten GE, Svendsen JSM, Stensen W. A synthetic antimicrobial peptidomimetic (LTX 109): stereochemical impact on membrane disruption. *J. Med. Chem.* 2011; **54**: 5786–5795. DOI: 10.1021/jm200450h
33 Stridh H, Cotgreave I, Müller M, Orrenius S, Gigliotti D. Organotin-induced caspase activation and apoptosis in human peripheral blood lymphocytes. *Chem. Res. Toxicol.* 2001; **14**: 791–798.
34 Engeland Mv, Nieland LJW, Ramaekers FCS, Schutte B, Reutelingsperger CPM. Annexin V-affinity assay: a review on an apoptosis detection system based on phosphatidylserine exposure. *Cytometry* 1998; **31**: 1–9.
35 Leuschner C, Hansel W. Membrane disrupting lytic peptides for cancer treatments. *Curr. Pharm. Design* 2004; **10**: 2299–2310.
36 Shai Y, Oren Z. From "carpet" mechanism to de-novo designed diastereomeric cell-selective antimicrobial peptides. *Peptides* 2001; **22**: 1629–1641. DOI: 10.1016/s0196-9781(01)00498-3
37 Chan WC, White PD. *Fmoc solid phase peptide synthesis—a practical approach*. Oxford university press: UK, 2002.
38 Brandl M. Liposomes as drug carriers: a technological approach. *Biotechnol. Annu. Rev.* 2001; **7**: 59–85.
39 Ingebrigtsen L, Brandl M. Determination of the size distribution of liposomes by SEC fractionation, and PCS analysis and enzymatic assay of lipid content. *AAPS PharmSciTech* 2002; **3**: 9–15. DOI: 10.1208/pt030207
40 *Maestro, version 9.2*. Schrödinger, LCC: New York, NY, 2011.
41 Jorgensen WL, Maxwell DS, Tirado-Rives J. Development and testing of the OPLS all-atom force field on conformational energetics and properties of organic liquids. *J. Am. Chem. Soc.* 1996; **118**: 11225–11236. DOI: 10.1021/ja9621760
42 Kaminski GA, Friesner RA, Tirado-Rives J, Jorgensen WL. Evaluation and reparametrization of the OPLS-AA force field for proteins via comparison with accurate quantum chemical calculations on peptides. *J. Phys. Chem. B* 2001; **105**: 6474–6487. DOI: 10.1021/jp003919d
43 *Desmond Molecular Dynamics System, version 2.2*. D.E. Shaw Research: New York, NY, 2009.
44 *Maestro-Desmond Interoperability Tools, version 2.2*. Schrödinger: New York, NY, 2009.
45 Bowers KJ, Chow E, Huafeng X, Dror RO, Eastwood MP, Gregersen BA, Klepeis JL, Kolossvary I, Moraes MA, Sacerdoti FD, Salmon JK, Yibing S, Shaw DE. Scalable algorithms for molecular dynamics simulations on commodity clusters. *Proceedings of the ACM/IEEE, SC 2006 Conference, 11–17* Nov. 2006, pp 43–43.
46 Berendsen HJC, Postma JPM, Gunsteren WFv, Hermans J. Interaction models for water in relation to protein hydration. In *Intermolecular Forces*, Pullman B (ed.). Reidel Publishing Company: Dordrecht; pp. 1981, 331–342.
47 Hoover WG. Canonical dynamics: equilibrium phase-space distributions. *Phys. Rev. A* 1985; **31**: 1695–1697.
48 Nosé S. A molecular dynamics method for simulations in the canonical ensemble. *Mol. Phys.* 1984; **52**: 255–268. DOI: 10.1080/00268978400101201
49 Martyna GJ, Tobias DJ, Klein ML. Constant pressure molecular dynamics algorithms. *J. Chem. Phys.* 1994; **101**: 4177–4190.
50 Darden T, York D, Pedersen L. Particle mesh Ewald: an N.log(N) method for Ewald sums in large systems. *J. Chem. Phys.* 1993; **98**: 10089–10092.
51 Tuckerman ME, Berne BJ, Rossi A. Molecular dynamics algorithm for multiple time scales: Systems with disparate masses. *J. Chem. Phys.* 1991; **94**: 1465–1469. DOI: 10.1063/1.460004
52 Ryckaert J-P, Ciccotti G, Berendsen HJC. Numerical integration of the cartesian equations of motion of a system with constraints: molecular dynamics of n-alkanes. *J. Comput. Phys.* 1977; **23**: 327–341. DOI: 10.1016/0021-9991(77)90098-5
53 Gottlieb HE, Kotlyar V, Nudelman A. NMR chemical shifts of common laboratory solvents as trace impurities. *J. Org. Chem.* 1997; **62**: 7512–7515.




  